Supporting Information

Reduced Graphene Oxide Layers Full of Bubbles for Electromagnetic Interference Shielding

Sufang Yang,[a, b] Zechao Tao,*[a, c] Xiangfen Li,[a] Jinxing Liu,[a] Qingqiang Kong,[a] Yelong Tong,[d] Junfen Li,[a] Zhanjun Liu, *[a, c, e]

[a] CAS Key Laboratory of Carbon Materials, Institute of Coal Chemistry, Chinese Academy of Sciences, Taiyuan, 030001, China

[b] University of Chinese Academy of Sciences, Beijing, 100049, China

[c] Dalian National Laboratory for Clean Energy, Dalian, 116023, China

[d] China Academy of Space Technology, Beijing, 100049, China

[e] Center of Materials Science and Optoelectronics Engineering, University of Chinese Academy of Sciences, Beijing, 100049, China

*Corresponding author. CAS Key Laboratory of Carbon Materials, Institute of Coal Chemistry, Chinese Academy of Sciences, Taiyuan, 030001, China

** Corresponding author. CAS Key Laboratory of Carbon Materials, Institute of Coal Chemistry, Chinese Academy of Sciences, Taiyuan, 030001, China

E-mail addresses: taozechao05@sxicc.ac.cn (Z. Tao), zjliu03@sxicc.ac.cn (Z. Liu)

Equations

1 Scherrer equation

$$L_c = \frac{K\lambda}{\beta_{002} \cos \theta_{002}} \tag{S1}$$

Where K is sample shape constant (Cu-target, 0.154 nm), λ is X-ray source wavelength, β is full width at half maximum of the (002) peak, and θ is the Bragg diffractive angle.

2 Cançadó equation

$$L_a = (2.4 \times 10^{-10})\, \lambda_{lasur}^{4} \left(\frac{I_D}{I_G}\right)^{-1} \tag{S2}$$

Where L_a is crystalline sizes, and λ_{laser} is wavelength (532 nm) of laser in Raman testing.

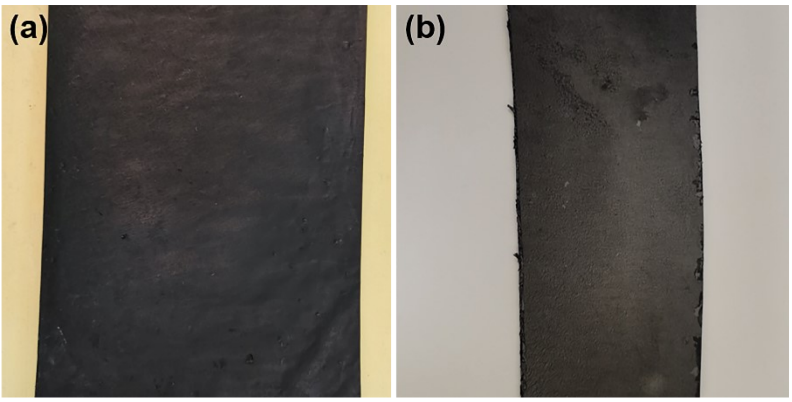

Fig. S1. Photograph of (a) GO-1VC, and (b) rGO-1VC-200.

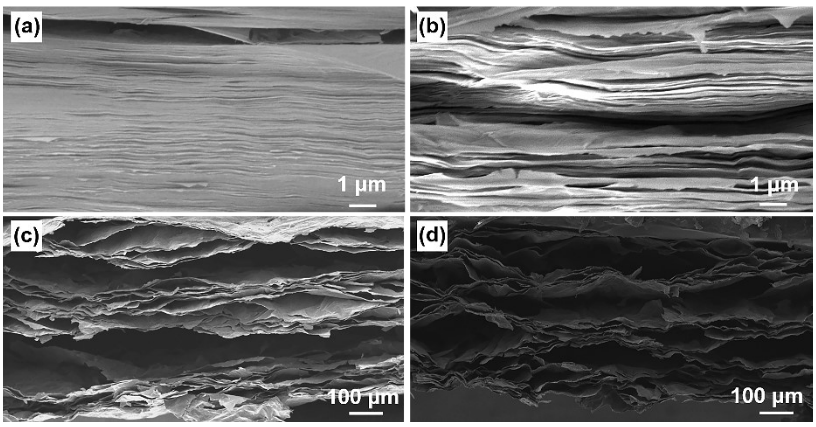

Fig. S2. SEM images of (a) GO, (b) rGO-90, (c) rGO-200, and (d) rGO-500 cross-sections.

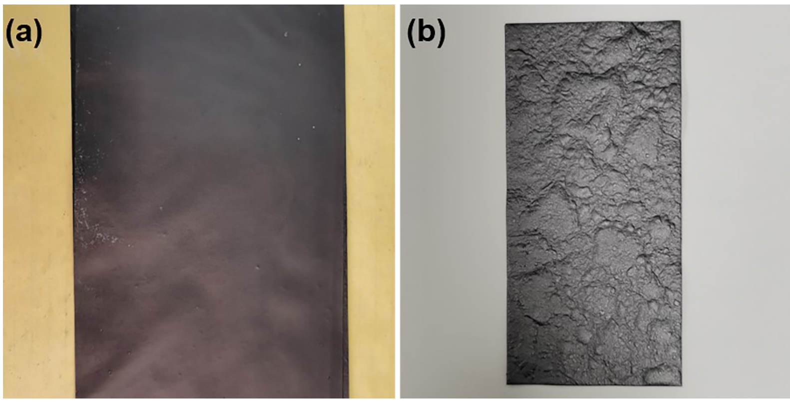

Fig. S3. Photograph of (a) GO and (b) rGO-200.

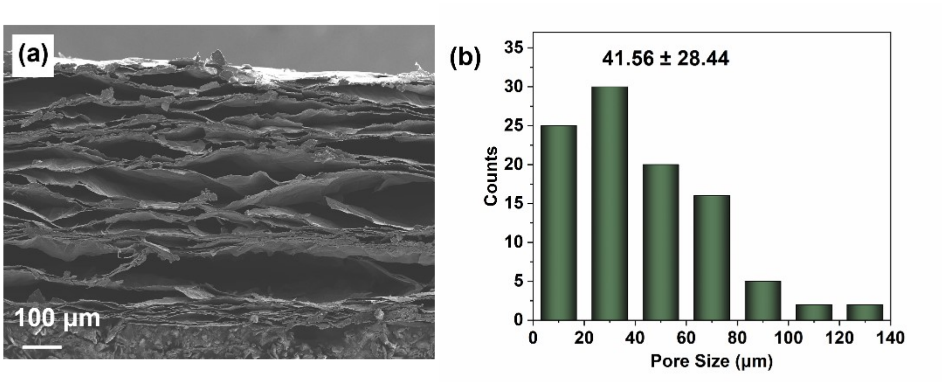

Fig. S4. (a) SEM image and (b)the pore size histograms of rGO-0.2VC-200.

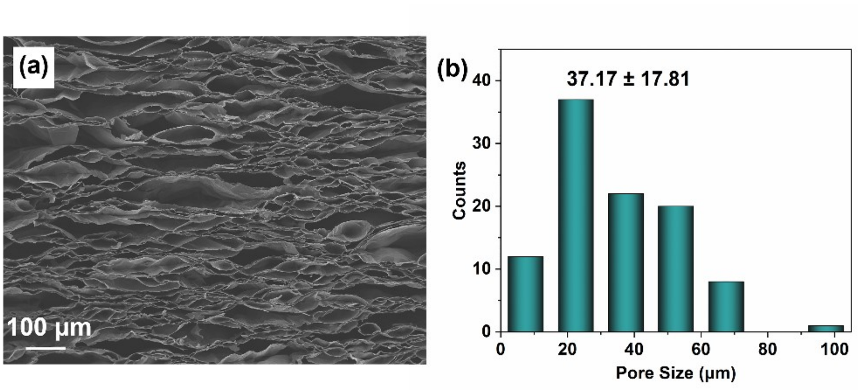

Fig. S5. (a) SEM image and (b) the pore size histograms of rGO-0.5VC-200.

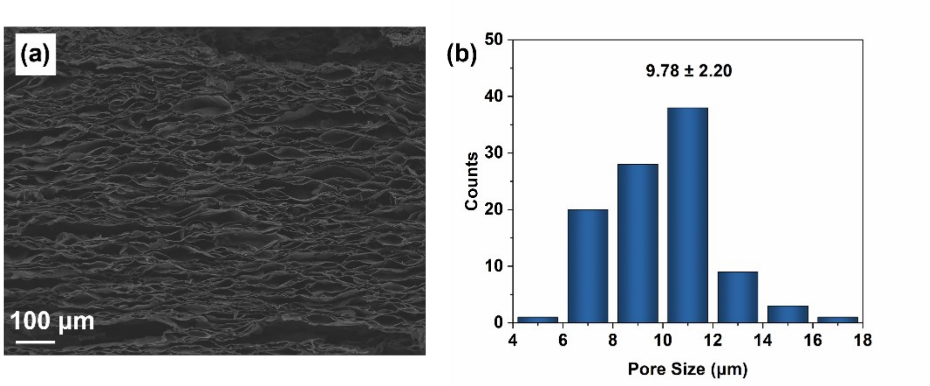

Fig. S6. (a) SEM image and (b) the pore size histograms of rGO-2VC-200.

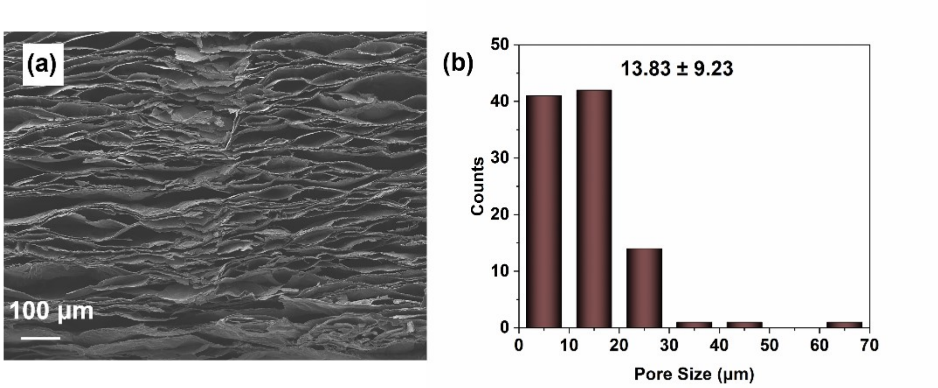

Fig. S7. (a) SEM image and (b) the pore size histograms of rGO-3VC-200.

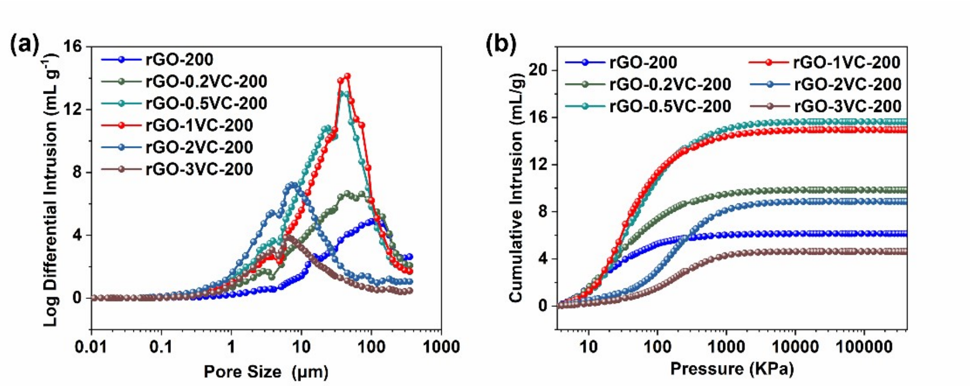

Fig. S8. (a) Pore diameter distribution curves and (b) mercury injection curves of rGO-xVC-200.

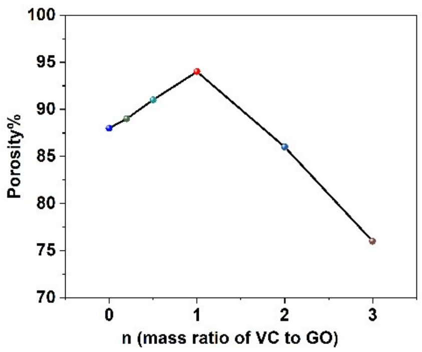

Fig. S9. Porosity of rGO-xVC-200.

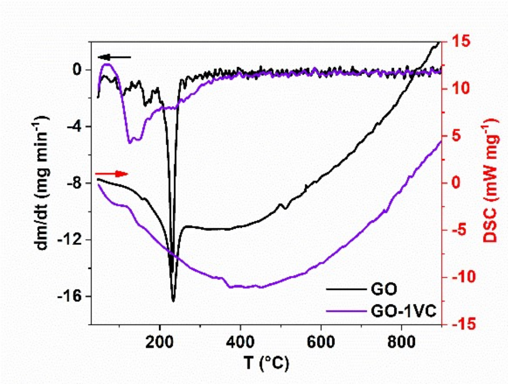

Fig. S10. The TG-DTG-DSC analysis of GO and GO-1VC.

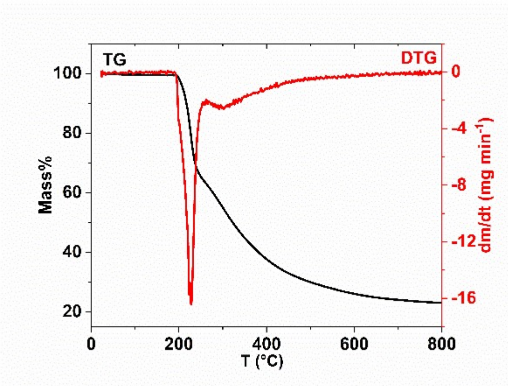

Fig. S11. The TG-DTG analysis of VC.

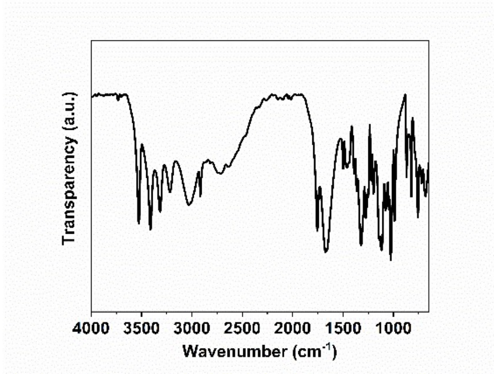

Fig. S12. The FT-IR of VC.

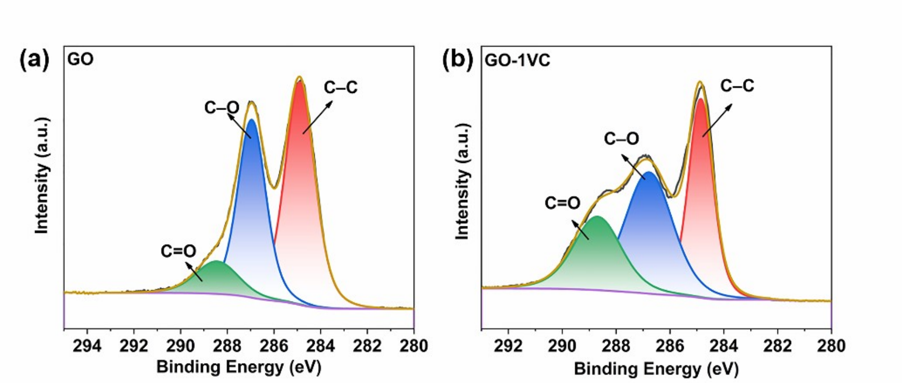

Fig. S13. C 1s XPS spectra of (a) GO and (b) rGO-1VC.

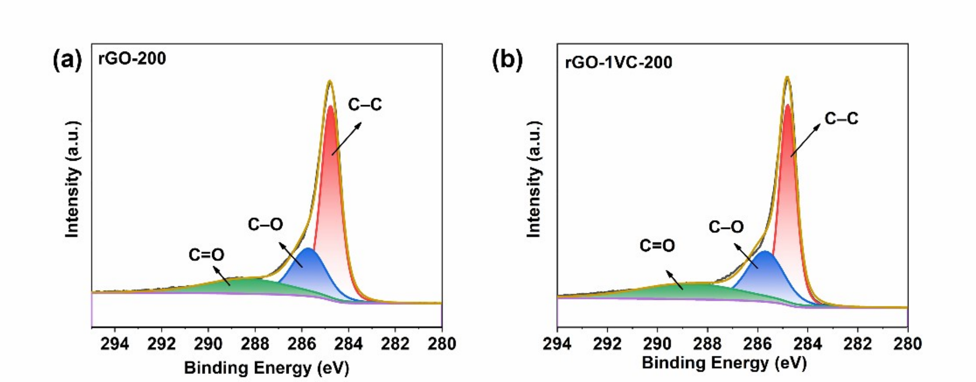

Fig. S14. C 1s XPS spectra of (a) rGO-200 and (b) rGO-1VC-200.

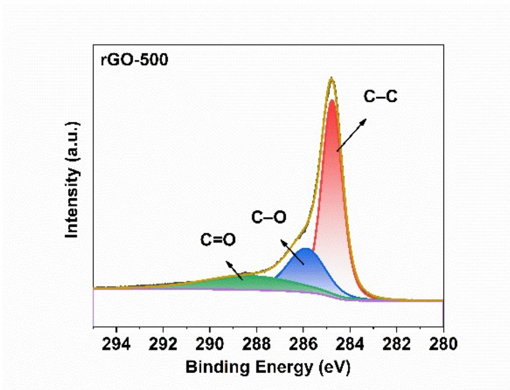

Fig. S15. C 1s XPS spectra of rGO-500.

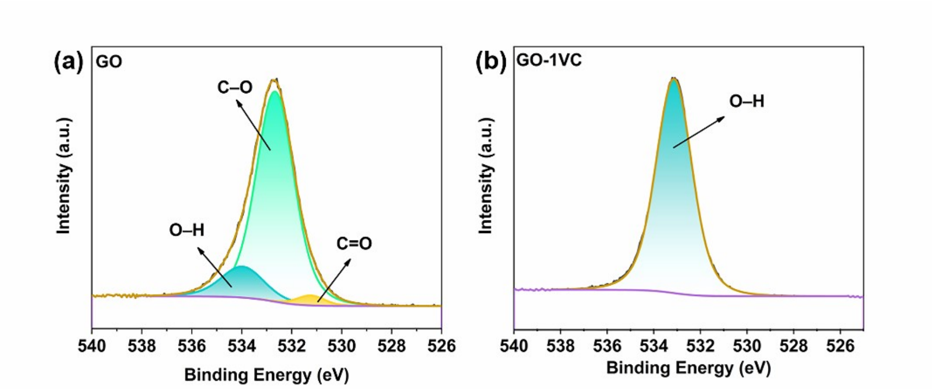

Fig. S16. O 1s XPS spectra of (a) GO and (b) GO-1VC.

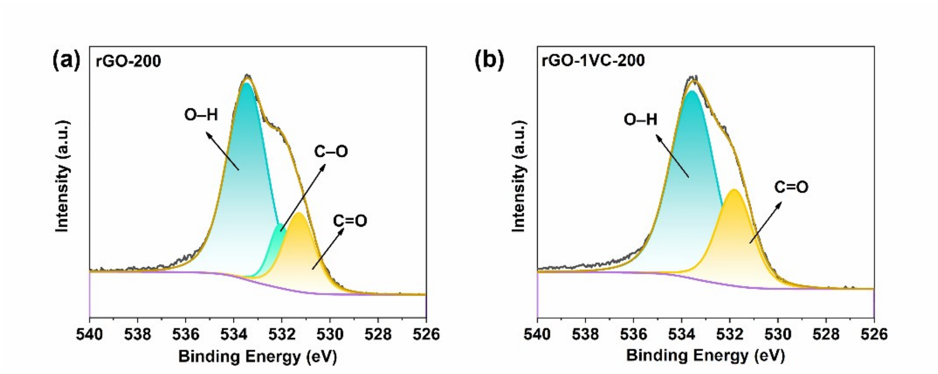

Fig. S17. O 1s XPS spectra of (a) rGO-200 and (b) rGO-1VC-200.

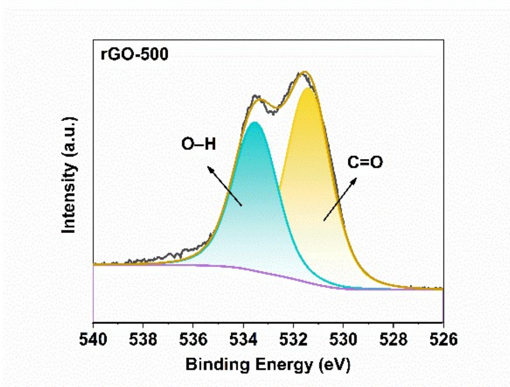

Fig. S18. O 1s XPS spectra of rGO-500.

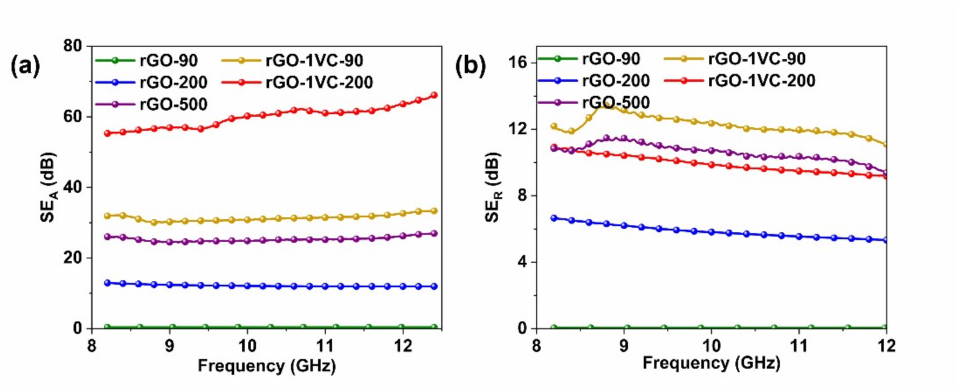

Fig. S19. (a) SE_A and (b) SE_R of rGO-90, rGO-200, rGO-500, rGO-1VC-90, and rGO-1VC-200.

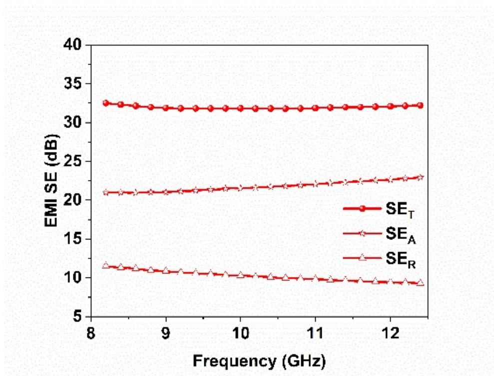

Fig. S20. The average SE values of rGO-1VC-200-C.

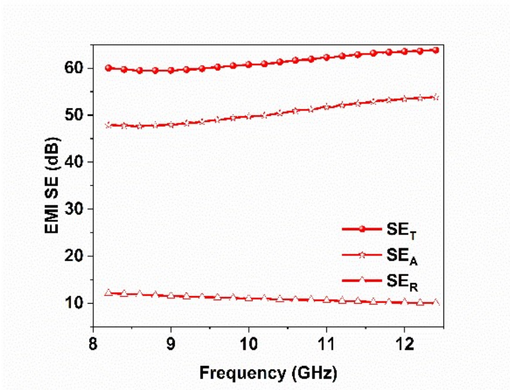

Fig. S21. The average SE values of rGO-1VC-200-P.

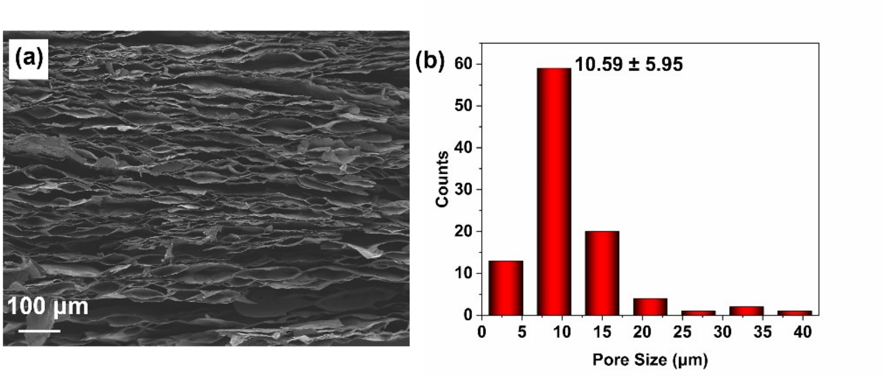

Fig. S22. (a-b) SEM image and the pore size histograms of rGO-1VC-200-P.

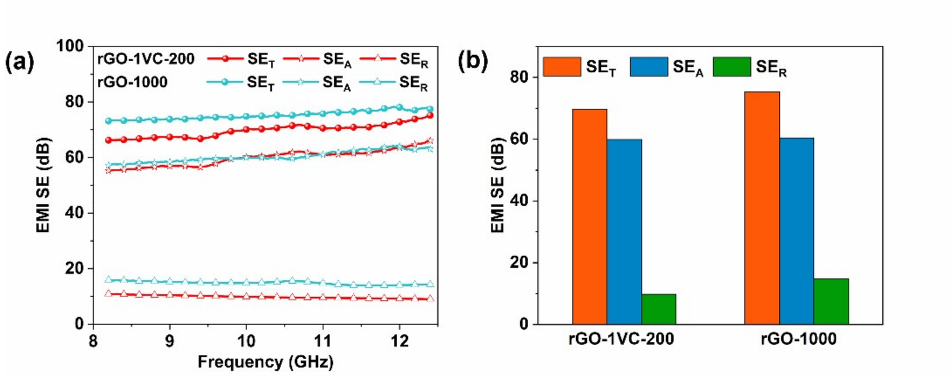

Fig. S23. The average SE values of rGO-1VC-200 and rGO-1000.

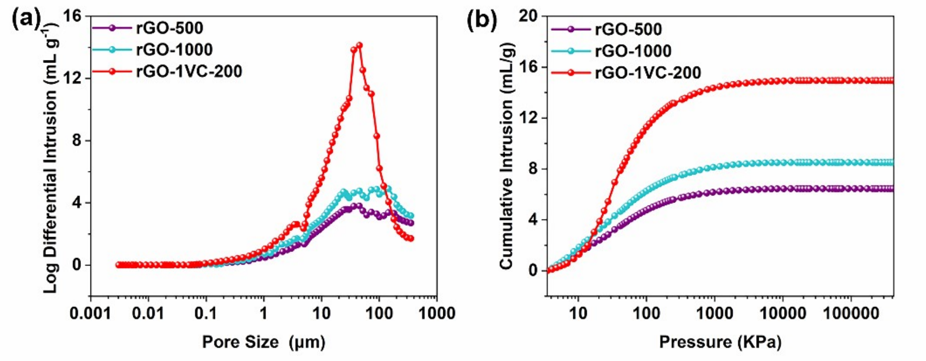

Fig.S24. (a) Pore diameter distribution curves and (b) mercury injection curves of rGO-500, rGO-1000 and rGO-1VC-200.

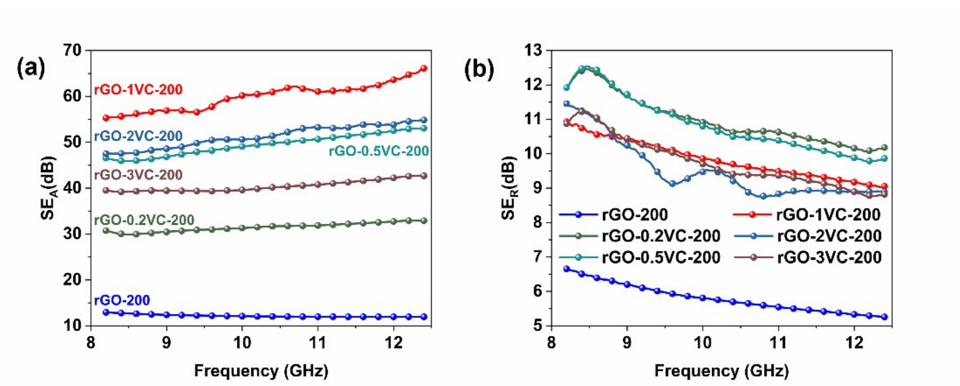

Fig. S25. (a) SE_A and (b) SE_R of rGO-xVC-200.

Table S1 Thickness and bulk density of all samples

Samples	Thickness (mm)	Density (g cm^{-3})
GO	0.080	1.40
rGO-90	0.100	1.27
rGO-200	0.380	0.20
rGO-500	0.400	0.15
GO-1VC	0.141	0.73
rGO-1VC-90	0.212	0.51
rGO-1VC-200	1.346	0.06
rGO-0.2VC-200	0.432	0.14
rGO-0.5VC-200	1.025	0.08
rGO-2VC-200	1.109	0.13
rGO-3VC-200	0.901	0.12

Table S2 Structural values of Raman and XRD spectra.

Samples	2 Theta (degree)	$d_{(002)}$ (Å)	FWHM (degree)	L_c (nm)	I_D/I_G	L_a (nm)
GO	13.74	6.44	0.61	134	1.42	13.54
rGO-90	14.88	5.95	0.85	95	1.56	12.32
rGO-200	20.64	4.30	2.82	29	1.80	10.68
rGO-500	24.90	3.57	0.91	90	1.78	10.80
GO-1VC	16.04	5.52	6.45	12	1.25	15.38
rGO-1VC-90	24.87	3.58	9.02	9	1.49	12.90
rGO-1VC-200	25.62	3.47	4.62	87	1.72	11.18

Table S3 Elemental analysis of all samples

Samples	Element content (wt%)					C/O
	N	C	H	S	O	
GO	0	48.09	2.42	0.58	41.38	1.16
rGO-90	0	64.02	1.48	0.31	40.08	1.60
rGO-200	0	76.69	0.63	0.13	20.72	3.70
rGO-500	0	86.91	0.75	0	11.27	7.71
GO-1VC	0	46.01	3.41	0.17	43.78	1.05
rGO-1VC-90	0	44.90	3.17	0.23	29.02	1.55
rGO-1VC-200	0	73.41	1.61	0	15.10	4.86

Table S4 The electrical conductivity and EMI SE of all samples.

Samples	Electrical conductivity (S cm^{-1})	SE_T (dB)	SE_A (dB)	SE_R (dB)	SE_T/ρ (dB cm^3 g^{-1})
GO	-	-	-	-	-
rGO-90	0.004	0.42	0.39	0.03	0.34
rGO-200	6.02	18	12	6	87
rGO-500	42.70	36	26	10	237
GO-1VC	10.64	-	-	-	-
rGO-1VC-90	22.47	13	31	12	85
rGO-1VC-200	60.61	70	60	10	1167
rGO-0.2VC-200	46.90	42	31	11	300
rGO-0.5VC-200	52.66	60	49	11	750
rGO-2VC-200	17.93	61	51	9	469
rGO-3VC-200	17.02	50	40	10	417

Table S5 EMI SE comparison of various shielding materials.

Number	Samples	The preparation methods	EMI SE (dB)	Density (g cm^{-3})	SET/ρ (dB cm^3 g^{-1})	Reference
1	rGO-1VC-200	Chemical reduction without template (200 °C)	70	0.06	1167	This work
2	MXene/RGO scaffolds	3D printing followed thermal annealing at 500 °C	79	0.145	483	1
3	$Ti_3C_2T_x$ MXene film	Thermal annealing at 500 °C	57.8	2.57	22.59	2
4	C_{60}/CD complex	Thermal annealing at 360 °C	53.52	1.914	28	3
5	CNF mat	The wet papermaking method	52-81	0.13-0.22	370-470	4
6	Multilayered MWNTs	Chemical vapor deposition (700 °C)	19.2	1.72	32.98	5
7	CNT film	High temperature at 1000 °C and acid treament	101.4	1.39	72.9	6
8	graphene film	HI reduction and annealing at 3000 °C	130	1.63	79.75	7

9	Graphene/carbon nanotubes	HI reduction and annealing at 2800 °C	75	1.06	70.75	8
10	CNF-PS foams	Sacrificial template method	20.51	0.62	33.1	9
11	CH-rGO foam	Freeze-drying strategy followed hydrazine monohydrate vapor reduction	42	0.061	688.5	10
12	CNT sponges	Chemical vapor deposition and vacuum-assisted impregnationwf	56	0.01	5480	11
13	MPBC-18	Thermal annealing (800 °C) and impregnation	95.67	0.32	298.97	12
14	Foamed Cu-Ni-CNT composite	Sacrificial template and electrophoretic deposition method	54.6	0.23	237.4	13
15	PIF-WS	One-pot liquid foaming process	3.8	0.016	216-249	14
16	SF-EP-CNT4	Wet-chemical deposition and foaming method	68.1	0.61	111.66	15
17	MWCNT/Ag NWs/MWCNT film	Vacuum-assisted filtration	72.1	0.97	74.33	16
18	PI/rGO foam	In situ polymerization, nonsolvent induced phase separation and thermal imidization	21	0.022	937	17
19	3D rGO-GNP	A facile foaming route (1500 °C)	94	1.1	85.5	18
20	PU/GO foam	Solution dip-coating and hydrazine monohydrate reduction	19..9~57.7	0.030	663.3~1923.3	19
21	CF/graphene aerogels	Freeze drying and annealed at 1000 °C	~42.5	0.0028	16890	20
22	TPU/RGO composite foams	Foaming method	21.8	~0.7	~31.14	21

Table S6 The EMI shielding performance of various shielding materials in a broad bandwidth.

Number	samples	Thickness (mm)	Density (g cm^{-3})	S-band (dB)	C-band (dB)	X-band (dB)	Ku-band (dB)	Reference
1	rGO-1VC-200	1.346	0.06	54	63	70	73	This work
2	SF-EP-CNT4	2	0.61	77	73	68	72	15
3	CF/graphene aerogels	2.83	0.0028	-	-	~43	~45	20
4	GR:1000	5	0.006	-	-	40		22
5	GF@PDMS	4.5	69.2	-	-	36		23
6	Graphene hybrid film	0.160	-	-	-	29	24	24
7	rGO composites	2	-	~7	~10	~8	~7	25
8	TPU/G film	0.050	-	-	~15	~18	~20	26
9	PMMA/CNT	0.57	-	-	-	~14	~18	27
10	Graphene foam	0.3	0.06	-	-	25	~27	28
11	NBR/GN	6	-	~46	~50	~70	-	29
12	APD MXene-based aerogels	2	18	-	-	65	67	30
13	C-MXene/SA-CNTfilms	0.009	-	-	-	60	~62	31
14	MS-based hydrogels	2	-	-	-	~47	~57	32

Reference

1 Y. Dai, X. Wu, L. Li, Y. Zhang, Z. Deng, Z.Z. Yu, H.B. Zhang, 3D printing of resilient, lightweight and conductive MXene/reduced graphene oxide architectures for broadband electromagnetic interference shielding, *J. Mater. Chem. A*, 2022, **10**, 11375-11385.

2 C. Xiang, R. Guo, S. Lin, S. Jiang, J. Lan, C. Wang, C. Cui, H. Xiao, Y. Zhang, Lightweight and ultrathin TiO_2-Ti_3C_2TX/graphene film with electromagnetic interference shielding, *Chem. Eng. J.*, 2019, **360**, 1158-1166.

3 K. Qian, S. Li, J. Fang, Y. Yang, S. Cao, M. Miao, X. Feng, C_{60} intercalating Ti_3C_2T MXenes assisted by γ-cyclodextrin for electromagnetic interference shielding films with high stability, *J. Mater. Sci. Technol.*, 2022, **127**, 71-77.

4 X. Hong, D.D.L. Chung, Carbon nanofiber mats for electromagnetic interference shielding, *Carbon*, 2017, **111**, 529-537.

5 D.W. Lee, H. Kim, J.H. Moon, J.H. Jeong, H.J. Sim, B.J. Kim, J.S. Hyeon, R.H. Baughman, S.J. Kim, Orthogonal pattern of spinnable multiwall carbon nanotubes for electromagnetic interference shielding effectiveness, *Carbon*, 2019, **152**, 33-39.

6 Y.J. Wan, X.Y. Wang, X.M. Li, S.Y. Liao, Z.Q. Lin, Y.G. Hu, T. Zhao, X.L. Zeng, C.H. Li, S.H. Yu, P.L. Zhu, R. Sun, C.P. Wong, Ultrathin Densified Carbon Nanotube Film with "Metal-like" Conductivity, Superior Mechanical Strength, and Ultrahigh Electromagnetic Interference Shielding Effectiveness, *ACS Nano*, 2020, **14**, 14134-14145.

7 E. Zhou, J. Xi, Y. Liu, Z. Xu, Y. Guo, L. Peng, W. Gao, J. Ying, Z. Chen, C. Gao, Large-area potassium-doped highly conductive graphene films for electromagnetic interference shielding, *Nanoscale*, 2017, **9**, 18613-18618.

8 H. Jia, Q.Q. Kong, X. Yang, L.J. Xie, G.H. Sun, L.L. Liang, J.P. Chen, D. Liu, Q.G. Guo, C.M. Chen, Dual-functional graphene/carbon nanotubes thick film: Bidirectional thermal dissipation and electromagnetic shielding, *Carbon*, 2021, **171**, 329-340.

9 Y. Yang, M.C. Gupta, K.L. Dudley, R.W. Lawrence, Novel carbon nanotube-polystyrene foam composites for electromagnetic interference shielding, *Nano Lett.*, 2005, **5**, 2131-4.

10 Y. Yuan, L. Liu, M. Yang, T. Zhang, F. Xu, Z. Lin, Y. Ding, C. Wang, J. Li, W. Yin, Q. Peng, X. He, Y. Li, Lightweight, thermally insulating and stiff carbon honeycomb-induced graphene composite foams with a horizontal laminated structure for electromagnetic interference shielding, *Carbon*, 2017, **123**, 223-232.

11 D. Lu, Z. Mo, B. Liang, L. Yang, Z. He, H. Zhu, Z. Tang, X. Gui, Flexible, lightweight carbon nanotube sponges and composites for high-performance electromagnetic interference shielding, *Carbon*, 2018, **133**, 457-463.

12 G. Wang, D. Lai, X. Xu, Y. Wang, Lightweight, stiff and Heat-Resistant Bamboo-Derived carbon scaffolds with gradient aligned microchannels for highly efficient EMI shielding, *Chem. Eng. J.*, 2022, **446**, 136911.

13 K. Ji, H. Zhao, J. Zhang, J. Chen, Z. Dai, Fabrication and electromagnetic interference shielding performance of open-cell foam of a Cu–Ni alloy integrated with CNTs, *Appl. Surf. Sci.*, 2014, **311**, 351-356.

14 J. Ma, K. Wang, M. Zhan, A comparative study of structure and electromagnetic interference shielding performance for silver nanostructure hybrid polyimide foams, *RSC Adv.*, 2015, **5**, 65283-65296.

15 Y. Xu, Y. Li, W. Hua, A. Zhang, J. Bao, Light-Weight Silver Plating Foam and Carbon Nanotube Hybridized Epoxy Composite Foams with Exceptional Conductivity and Electromagnetic Shielding Property, *ACS Appl. Mater. Interfaces*, 2016, **8**, 24131-24142.

16 Z. Wang, Q.Q. Kong, Z.L. Yi, L.J. Xie, H. Jia, J.P. Chen, D. Liu, D. Jiang, C.M. Chen, Electromagnetic interference shielding material for super-broadband: multi-

walled carbon nanotube/silver nanowire film with an ultrathin sandwich structure, *J. Mater. Chem. A*, 2021, **9**, 25999-26009.

17 Y. Li, X. Pei, B. Shen, W. Zhai, L. Zhang, W. Zheng, Polyimide/graphene composite foam sheets with ultrahigh thermostability for electromagnetic interference shielding, *RSC Adv.*, 2015, **5**, 24342-24351.

18 J. Li, X. Zhao, W. Wu, X. Ji, Y. Lu, L. Zhang, Bubble-templated rGO-graphene nanoplatelet foams encapsulated in silicon rubber for electromagnetic interference shielding and high thermal conductivity, *Chem. Eng. J.*, 2021, **415**, 129054.

19 B. Shen, Y. Li, W. Zhai, W. Zheng, Compressible Graphene-Coated Polymer Foams with Ultralow Density for Adjustable Electromagnetic Interference (EMI) Shielding, *ACS Appl. Mater. Interfaces*, 2016, **8**, 8050-8057.

20 Y.J. Wan, P.L. Zhu, S.H. Yu, R. Sun, C.P. Wong, W.H. Liao, Ultralight, super-elastic and volume-preserving cellulose fiber/graphene aerogel for high-performance electromagnetic interference shielding, *Carbon*, 2017, **115**, 629-639.

21 Q. Jiang, X. Liao, J. Li, J. Chen, J. Yi, Q. Yang, G. Li, Flexible thermoplastic polyurethane/reduced graphene oxide composite foams for electromagnetic interference shielding with high absorption characteristic, *Composites Part A*, 2019, **123**, 310-319.

22 M. González, J. Baselga, J. Pozuelo, Modulating the electromagnetic shielding mechanisms by thermal treatment of high porosity graphene aerogels, *Carbon*, 2019 **147**, 27-34.

23 H. Li, L. Jing, Z.L. Ngoh, R.Y. Tay, J. Lin, H. Wang, S.H. Tsang, E.H.T. Teo,

Engineering of High-Density Thin-Layer Graphite Foam-Based Composite Architectures with Superior Compressibility and Excellent Electromagnetic Interference Shielding Performance, *ACS Appl. Mater. Interfaces*, 2018, **10**, 41707-41716.

24 L. Ma, Z. Lu, J. Tan, J. Liu, X. Ding, N. Black, T. Li, J. Gallop, L. Hao, Transparent Conducting Graphene Hybrid Films To Improve Electromagnetic Interference (EMI) Shielding Performance of Graphene, *ACS Appl. Mater. Interfaces*, 2017, **9**, 34221-34229.

25 B. Wen, X.X. Wang, W.Q. Cao, H.L. Shi, M.M. Lu, G. Wang, H.B. Jin, W.Z. Wang, J. Yuan, M.S. Cao, Reduced graphene oxides: the thinnest and most lightweight materials with highly efficient microwave attenuation performances of the carbon world, *Nanoscale*, 2014, **6**, 5754-61.

26 B. Shen, Y. Li, D. Yi, W. Zhai, X. Wei, W. Zheng, Strong flexible polymer/graphene composite films with 3D saw-tooth folding for enhanced and tunable electromagnetic shielding, *Carbon*, 2017, **113**, 55-62.

27 K. Hayashida, Y. Matsuoka, Electromagnetic interference shielding properties of polymer-grafted carbon nanotube composites with high electrical resistance, *Carbon*, 2015, **85**, 363-371.

28 B. Shen, Y. Li, D. Yi, W. Zhai, X. Wei, W. Zheng, Microcellular graphene foam for improved broadband electromagnetic interference shielding, *Carbon*, 2016, **102**, 154-160.

29 A.A. Al-Ghamdi, A.A. Al-Ghamdi, Y. Al-Turki, F. Yakuphanoglu, F. El-Tantawy,

Electromagnetic shielding properties of graphene/acrylonitrile butadiene rubber nanocomposites for portable and flexible electronic devices, *Composites, Part B*, 2016, **88**, 212-219.

30 N. Wu, Y. Yang, C. Wang, Q. Wu, F. Pan, R. Zhang, J. Liu, Z. Zeng, Ultrathin Cellulose Nanofiber Assisted Ambient-Pressure-Dried, Ultralight, Mechanically Robust, Multifunctional MXene Aerogels, *Adv. Mater.*, 2022, e2207969.

31 B. Li, Y. Yang, N. Wu, S. Zhao, H. Jin, G. Wang, X. Li, W. Liu, J. Liu, Z. Zeng, Bicontinuous, High-Strength, and Multifunctional Chemical-Cross-Linked MXene/Superaligned Carbon Nanotube Film, *ACS Nano*, 2022, **16**, 19293-19304.

32 Y. Yang, N. Wu, B. Li, W. Liu, F. Pan, Z. Zeng, J. Liu, Biomimetic Porous MXene Sediment-Based Hydrogel for High-Performance and Multifunctional Electromagnetic Interference Shielding, *ACS Nano*, 2022, **16**, 15042-15052.